Journal of Ovonic Research Vol. 20, No. 6, November - December 2024, p. 851 - 865

Synthesis and characterization of SnO_2/porous silicon hybrid nanostructures for gas sensing

M. I. Ismael, G. G. Ali *, A. T. Zakar
Physics Department, College of Education for Pure Science, University of Mosul, Iraq

In this work, Tin oxide SnO_2 hybrid structures were deposited on porous silicon substrates via spray pyrolysis method. The impact of the current density changes ranging from 5- 15 mA/cm^2 with HF concentration of 18% was investigated at fixed substrate temperature of 250C^o. The XRD analysis for nanostructures revealed the presence of tetragonal structure of SnO_2. The Scanning electron Microscope (SEM) images showed the sponge-like structure of PSi with grooves and cavities following the deposition of SnO_2 on the substrate. It can be seen, the grain diameter arrangement of the SnO_2 was found to be in the range from 42–64 nm. The I-V characteristics showed that the resistance raises with the current density of the SnO_2/porous silicon. The optical results refers that the absorption of SnO_2 nanostructure increases with the number of spraying times for values of (10,15 and 20) respectively. Moreover, the results also revealed a degradation of the energy gap from 3.3 to 2.82eV at the same spraying values. The higher sensitivity was found around 49.35% at etching current density of 15mA/cm^2. The structure quality of the SnO_2/PSi provides the possibility of using such structures in the high-quality sensors.

(Received October 2, 2024; Accepted December 6, 2024)

Keywords: Tin oxide, Porous silicon, XRD, FESEM and gas sensor

1. Introduction

Tin oxide (SnO_2) has one of the most extensive attention material due to its use in various important applications in semiconductor specially in optical devices such as antireflection coating-gas sensors, chemical filters, solar cells, and photodetectors [1]. The SnO_2 is a wide band gap semiconductor 3.6 eV and has a high conductivity due to structural defects at the crystal structure as well as the presence of oxygen vacancies (VO) such as tin interstitial in its rutile tetragonal structure which affect as donors in the conduction band level [2]. The SnO_2 thin films have been deposed by several methods such as spray pyrolysis, sol-gel, physical vapor deposition (PECVD), sputtering and chemical bath deposition (CBD) [3]. Spray pyrolysis is a straight forward, simple and inexpensive method. The advantages of such approach in the fabrication and investigation of SnO_2 comes from their ability of producing high crystallinity, selective deposition, and high purity structures. In the recent technological applications, porous silicon and its derivative material have become a significant candidate in many fabrication fields [4,5]. Porous silicon is a complex structure containing a group of pores shifted by thin pillars with nano-diameter crystalline Si. Moreover, the mechanical and chemical stability as well as the compatibility with the current technological application provided the possibility of using porous silicon in the various fields such as photovoltaic devices, waveguides, chemical sensors, biological sensors [6,7,8]. The strong absorbability of the Psi and large internal configuration of surface area and makes it an appropriate material to accommodate SnO_2 thin film. The larger surface area of porous silicon (107 times larger than that of bulk) enhances the interaction between the silicon surface and gas particles which in turn boosts the sensitivity and provides the possibility by detection gas sensor [9,10]. In addition, porous silicon parameters such as porosity, structure and thickness can be precisely controlled. This can be achieved by fine tuning of the preparation conditions such as current

* Corresponding author: dr.ghazwan39@uomosul.edu.iq
https://doi.org/10.15251/JOR.2024.206.851

density, etching time and acid solution. This in turn provides the possibility of precise determination of the optical properties of the structure. The sensor mechanism of Tin dioxide is classified as material kind in which the oxygen adsorption and the grain size surface states have a important effect in the process. The deposition of SnO_2 on the porous silicon improves the morphological characteristics compared to bulk counterpart [11,12,13]. The combination of high - quality SnO_2 films and PSi layers are significantly important due to a large matching of lattice constants and thermal expansion coefficients. This work evaluates the morphological, and electro - optical properties of Tin oxide nanostructure deposed on porous silicon as a candidate in the gas sensing applications.

2. Experimental method

2.1. Preparation details of porous silicon

Porous silicon samples of p-type semiconductor with (111) oriented of 350-$^{+}$25µm thickness and a resistivity of 0.01–4 ohm. cm was carried out using electrochemical etching method. Silicon samples were immersed with alcohol and methanol solution by an ultrasonic bath at 15 min. The crystalline silicon samples were immersed with water solation and dried with Nitrogen flux. Then, the samples were put in composition solution (16%HF) and ethanol (99%). An anodized cell was made of Teflon, the contain a plastic O-ring of 2 cm^2 size to control of the solution from leaking out of cell. The set up consist of two regions, the first one is a circle metal kept under the silicon wafer and the second one is a gold mash represents the upper electrode which is immersed in the HF solution as shown in the Figure 1a. The process was achieved for 10 min also, we used different current density at 5,10 and 15 mA cm^2 respectively.

2.2. Synthesis and deposition of SnO_2

Tin dioxide was prepared using the ratio of mixed of $SnCl_2{\cdot}5H_2O$ (1.4 g, 0.1 mol) and NaOH (0.4 g, 0.1 mol). The mixture was kept in deionized water solutions and deposited on p-Si substrates using spray chemical approach. The acetate solution was stirred for 45 min using magnetic stirrer and heated up to 80^{o} C for two hours. The mixture then deposed on the substrates using spray chemical at 350◦C, 7.5 atmospheric pressure and spray steps 10 ,15 and 20 respectively. The time intervals between each spray were fixed to be 10 seconds as shown the Figure1b. The interaction of the process can be described by the following equation:

$$SnCl_4{\cdot}5H_2O + 4NaOH \rightarrow 4NaCl + 7H_2O + SnO_2 \quad (1)$$

The thickness of the films can be evaluated by the gravimetric process based on the following expression:

$$t = \Delta m / \rho A \quad (2)$$

where t is the film thickness, Δm is the weight difference before and after deposition, ρ is the density of Si film (2.32 gm/cm^3) and A is the surface area of the sample. Similarly, the thickness of the SnO_2 can be also estimated following the same procedure.

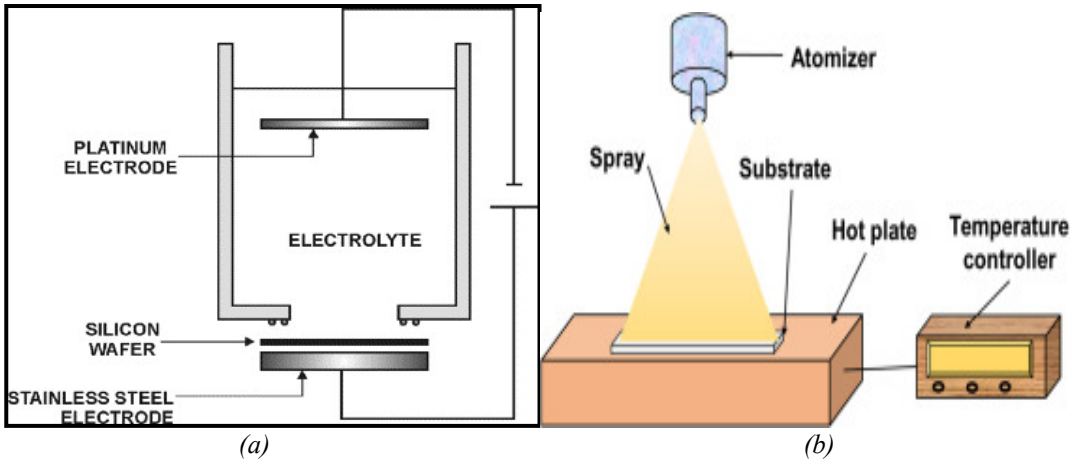

Fig. 1. diagram of set up (a) Anodization cell of porous silicon , (b) Spraypyrolysis method.

2.3. Setup gas-sensing

The performance of gas sensor SnO_2/PSi hetrostructure was studied by using measurement the change in the resistivity of the film with respect to the different operating temperature (50,100,150,200 and 250 °C) at fixed 60 pmm of NO_2 gas flue. Figure 2 illustrates the sensing system used to investigate the sensing response of the samples. The system encompasses the system encompasses fabricated stainlesssteel chamber with a volume of 260 cm^3, Power source, Multimeter with inlet and outlet sections to fill and evacuate the gases. The heating plate connected to the temperature controller was employed to controller sample temperature. A computer controlled keithley 2400 (USA) measurement was used to observed the data. The gas response of the sensor was calculated using the relation:

$$S\% = \frac{G_{air} - G_{gas}}{G_{air}} \times 100\% \quad (3)$$

where G_{air} and G_{gas} Where G_{gas} and G_{air} are resistances of gas sensing and air respectively.

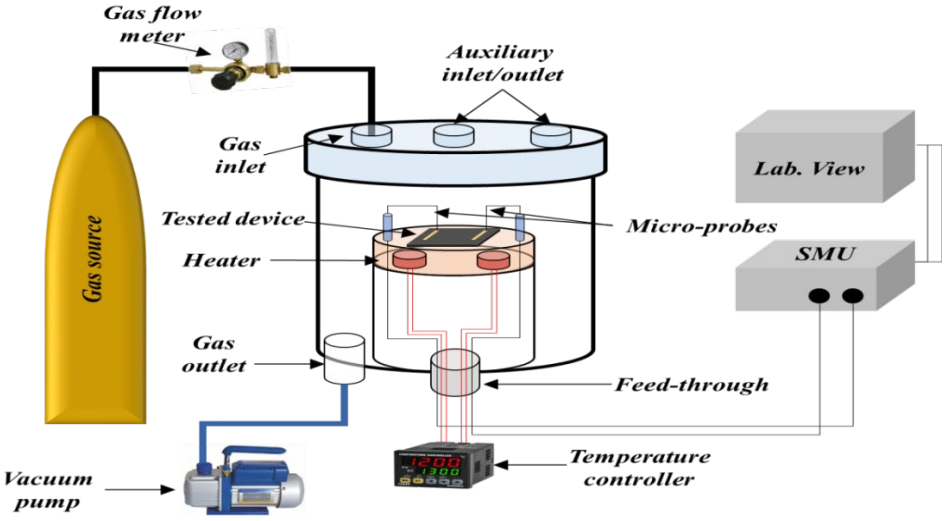

Fig. 2. Diagram of setup gas sensor.

3. Results and discussion

The X-ray diffraction (XRD) analysis was measured of crystallographic structure of thin films. The crystal structure of the pure SnO_2 was investigated using XRD pattern as in Figure 3(a). To study crystallographic structure of the substrate, the patterns of XRD analysis was measured as shown in the figure 3(a). The indicted peaks correspond to the lattice tetragonal structure as rutile type of Tin dioxide of (110), (101), (200) and (211) planes at $2\theta \cong 31.7^{\circ}$, 32.8°, 46.5° and 52.2° respectively. The results well matched the standard card (JCPDS, 41-1445) [14] indicating the high purity of the formed Tin dioxide. The SnO_2/porous silicon nanostructure were investigate using XRD analysis as shown in the figure 3(b,c and d). The results also exhibited that hediffraction peaks are broadening with increasing current density which could cause a reduce in the particle size as indicated in the table 1. The highest peak of PSi (111) was observed at 28.3º and other peaks were noticed at 26.8 º and 31. 3 º of CuS corresponding to (110) and (101) planes respectively [15,16]. Consequently, it can be seen, the pattern of the SnO_2/PS layer keeps crystalline region. On the other side, the diffraction angle may be slightly shifted to a smaller values due to influence of stress which can be act to a little expanded in lattice vibration. The grain size L is evaluated using Scherer's formula [17]:

$$L = \frac{k\lambda}{B\cos\theta} \tag{4}$$

where β refers to the half maximum (FWHM), θ indicates to the peak of Bragg angle, λ is symbolized to the wavelength of XRD (0.1543 nm) and k is the Scherrer constant.

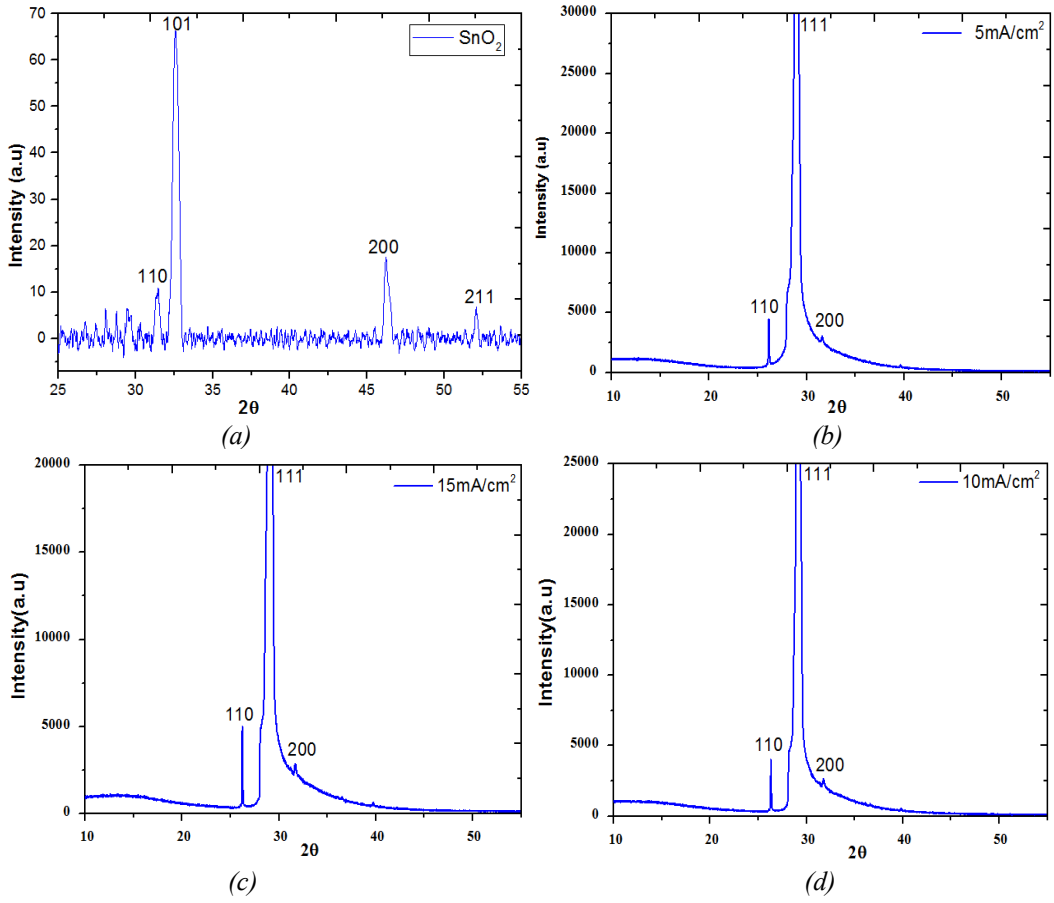

Fig. 3. XRD analysis for (a) SnO_2, (b) SnO_2/PSi at current density 5mA/cm^2, (c) SnO_2/PSi at current density 10mA/cm^2, (d) SnO_2/PSi at current density 15mA/cm^2.

Table 1. Parameters of inter-plane distance, FWHM, crystallites size of SnO_2/PSi with various s fixed current at 5,10 and 15 mA/cm^2.

Sample	Current density(mA/cm^2)	L (nm)	FWHM (deg)	d (A^o)
Pure SnO_2	-	0.060	0.0759	3.410
		0.6798	0.3483	3.148
		0.34814	0.206	3.124
		0.05293	0.0828	3.08
SnO_2/Porous silicon	5	0.98027	0.3133	3.141
		1.5189	0.6099	3.1700
		1.2661	0.7342	2.755
SnO_2/Porous silicon	10	0.5667	0.9226	2.819
		0.4112	1.4552	1.354
		0.7324	0.5904	1.5213
SnO_2/Porous silicon	15	0.4665	1.1556	1.3544
		0.3126	1.703	1.311
		0.1339	3.998	1.253

3.1. Scanning electron microscope (FESEM)

Figure 4(a) shows FESEM images of the porous silicon at current density 5 mA/cm^2. It obvious that the PSi surface has a network as sponge -structure configuration and a large number of pores overlap the walls. The pore sizes rise with etching current.

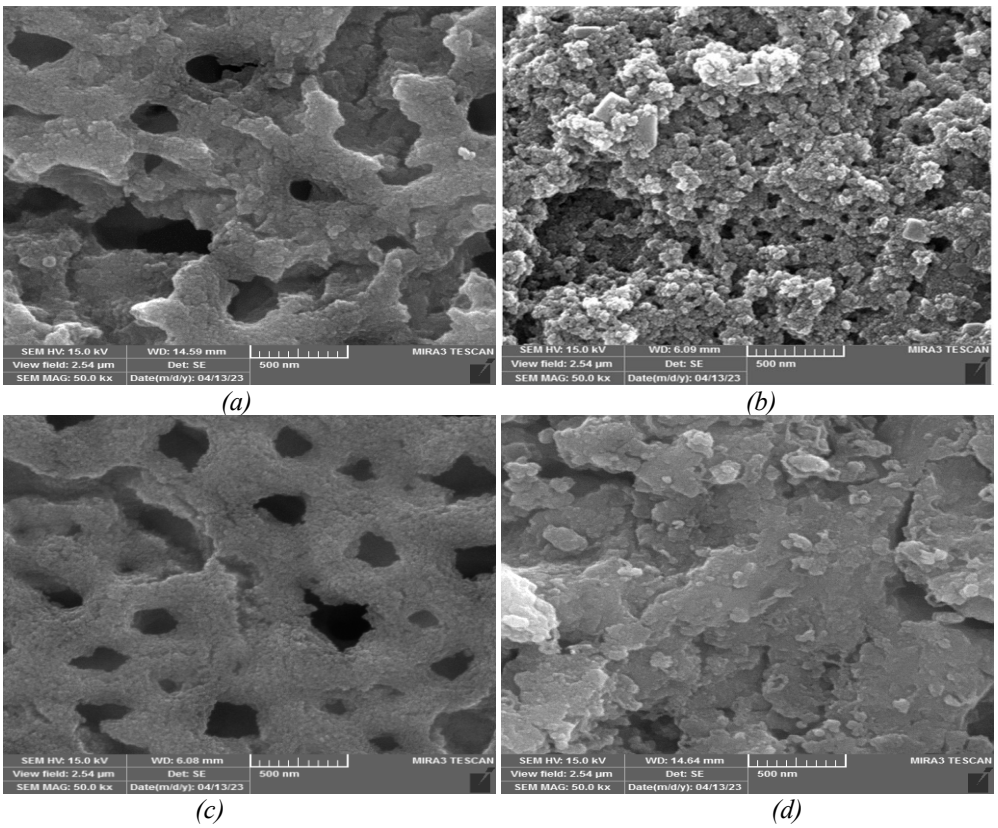

Fig. 4. Top surface of FESEM of (a) porous silicon at current density 5mA/cm^2, (b) SnO_2/PSi at current density 5mA/cm^2 , (c) porous silicon at current density 15mA/cm^2, (d) SnO_2/PSi at current density 15mA/cm^2.

The pore sizes rise with rising etching current due to the extra continuous chemical process in HF solution and then obtain the number of holes at the surface as illustrated in the Figure 4(c). Figure 4 (b and d) illustrate the typical top-view of the SnO_2/porous silicon nanostructures at concentration of 0.1M with current density 5 and 15 mA/cm^2 respectively. It can be also seen that the SnO_2NPs are randomly covering partial or completely filling pores at the surface. This leads to enhance the nucleation growth of SnO_2 thin films during the deposition process. The SnO_2 nanoparticles are quite homogeneous with the presence some grooves and cavities. The nano-range size arrangement of the SnO_2 nanostructures is 42–64 nm. It should be noted here that the chemical dissolution does not depend potential but on the current density and the total surface area of the PSi [18,19]. This in turn increases the thickness of the sample as shown in the Figure5(a). The figure 5(b) exhibits that the thickness of SnO_2 NPs is also increased with number of sprays.

3.2. UV-spectrophotometer

The optical analysis of the SnO_2 NPs was investigated using (UV-Vis Spectrophotometer) at ratio 0.1M and number of sprays (10,15 and 20) respectively. The absorption spectra of the visible region were represented as Figure 6a. The absorption patterns of the deposited film decrease sharply after λ=360 nm. These results indicate that the absorption of SnO_2 NPs raised with a number of spray (10,15 and 20). This could be due to the breakup of bonding on the SnO_2 surface, which acts to a raise the absorption process [20,21]. The number of spraying yields defect accumulation increased. These defects introduce absorption bands or color centers in photonic devices that significantly changes the optical properties of the materials. Figure 6b represents the absorption coefficient (α) of SnO_2 NPs calculated using Beer Lambert's formula [22]:

$$\alpha = 2.312\,\frac{A}{t} \tag{5}$$

where t refers to the film thickness. It can be observed that the absorption coefficient reduces with raising wavelength while this not the case with increasing the number of sprays, where the absorption increases. The high value of the absorption coefficient ($\alpha \geq 10^4$ cm^{-1}) refers to the possibility of direct transitions.

Figure 6c shows the reflectance spectrum of SnO_2 thin film calculated using the following expression:

$$R = 1 - (T + A) \tag{6}$$

The symbol A indicates the absorption and T refers to the transmission. It can be seen that reflection reduces with increasing wavelength. The figure also shows that the reflectance enhances with number of sprays, which could be attributed to photon absorption by the SnO_2 thin films.

Figure 6d indicates the curves between $(\alpha h\nu)^2$ and energy of photon ($h\nu$) of SnO_2 film. The energy gap reduction can be resultant to the interface band transition creating localized oxygen defects and the extra electrons generated by the n-type SnO_2. The energy gap (Eg) could be calculated by Tauc equation:

$$\alpha h\nu = B(h\nu - E_g)^r \tag{7}$$

The symbolized B indicates to the constant value whereas αrefers to the absorbance coefficient and r refers to the two types of transition (direct transition and indirect transition) respectively. The results exhibit that the energy gap reduces with number of sprays 3.3, 3. 1, 2.82 eV at number of sprays (10,15 and 20) respectively. the data obtained in this study are in a good agreement with publication works for SnO_2 NPs deposed by other process [23,24].

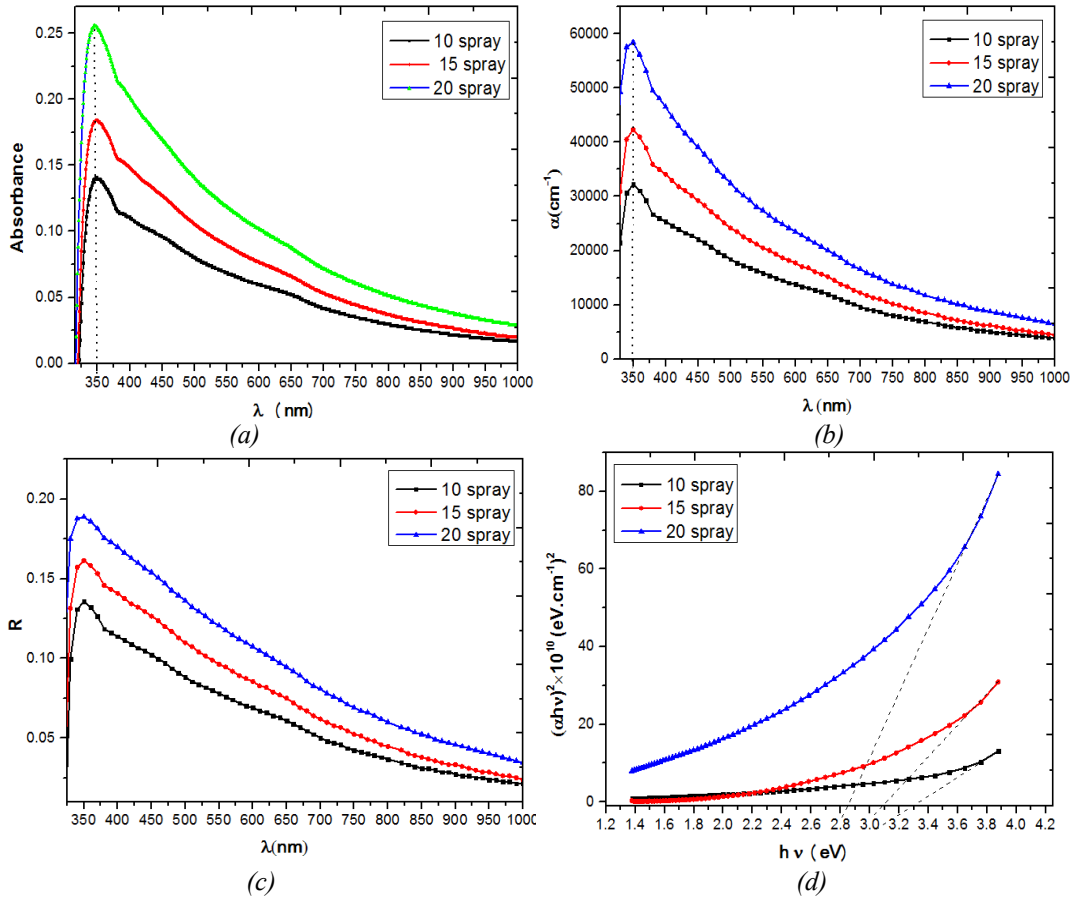

Fig. 6. (a) Absorption, (b) Absorption coefficient , (c) Reflective index, (d) Calculation of energy gap of SnO_2 films number of spray 10,15 and 20 deposited on glass substrate.

3.3. I-V measurements

Figure (7) shows the I-V measurements of SnO_2 deposed on PSi layers at different current densities (5, 10 and 15 min) respectively. The I-V characteristics revealed that the Schottky diode behavior in the hybrid framework was presented of with rectification properties. At low forward voltages, the forward current is small which can be attributed to the interface between SnO_2/PSi Besides, the presence of the crystal defect which control the current generation mechanism. Furthermore, increasing of the current circuit is observed of high values of voltage because of increase in the electron-hole generation. Without a doubt, the higher values of voltage may be attributed to the high reverse current generated by minority carriers, and, Then, higher electron-hole separation probability. The change in the I-V parameters is depended on the etching time. As the pore size raises with increasing the etching time. Importantly, increasing of the resistivity of the porous Si due to the trapped carriers at the pore wall [25,26]. To determine resistivity of the PSi, the following expression can be employed:

$$\rho_{PSi} = \frac{dV}{dJ.dpsi} \tag{8}$$

where $\boldsymbol{\rho_{PSi}}$ refers to layer resistivity, dV/dJ represents the slope at the omic part of I-V characteristic and d refers to the PSi thickness. As can be also seen that the resistivity enhances at longer etching times due to the carrier capturing between PSi/c-Si interface. To calculate the ideality factor (n) as well as barrier height (ΦB), the following equation can be used:

$$n = \frac{q}{KT}\left[\frac{d(LnI)}{dV}\right]^{-1} \tag{9}$$

$$\Phi_B = \frac{k_B T}{q}\ln\left(\frac{A^{**}T^2}{J}\right)$$

(10)

where $[\frac{d(LnI)}{dV}]^{-1}$ is the slope at the omic region of (I-V) plots, J represents the current density while k_B and A** are Boltzmann's constant and the Richardson's constants respectively.

Table 1 illustrates the extracted parameters values of the SnO_2/PSi hybrid structures.

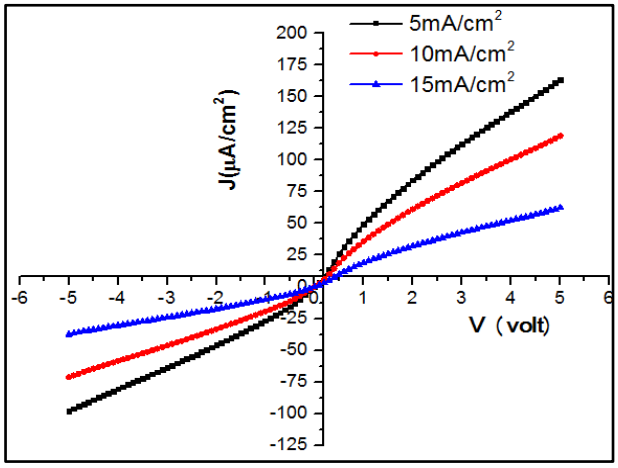

Fig. 7. I-V measurements of SnO_2/PSi at current density 5,10 and 15 mA/cm^2.

Table 2. Parameters of saturation current, ideality factor, barrier height and resistivity for current density (5, 10 and 15 mA/cm^2) of SnO_2/PSi at concentration 0.1M.

Current density(mA/cm^2)	J_s (mA/cm^2)	n	φB (eV)	(Ω.cm) ρ
5	13.25	2.62	0.623	1.77×10^5
10	7.82	2.74	0.675	3.53×10^6
15	1.92	2.82	0.73	5.7×10^7

3.4. Sensitivity of SnO_2/PSi

Figures 8, 9 and 10 (a,b and c) show the resistance (kΩ) with time (sec) of SnO_2/PSi hetrostructures at operating temperatures (50 ^{0}C ,100 ^{0}C and 150 ^{0}C) for fixed NO_2 gas concentration (50 ppm) and etching current densities (5,10 and 15 mA/cm^2) respectively . It is observed that the resistance of SnO2/PSi NPs increases with rising the temperature. [27]. This can be understood from the fact that the increase in surface temperature of SnO_2/PSi thin film yields wider depletion layer and higher resistance. The figure also indicated that the film resistance develops with the etching current which due to the raise in the interactivity of material with gas molecules concentration). Figure 11 represents the sensitivity of SnO_2/PSi heterojunction as NO_2 composite ratio (50ppm) at operating temperatures 50 ^{0}C, 100 ^{0}C, 150 ^{0}C, 200 ^{0}C and 250^{o}C respectively. It is observed from the figure that the substrates showed a good response with increasing etching current density because of increase of the exposed material of sample [28]. It should be noted here that the creation of Schottky barrier in a depletion region at SnO_2/PSi interface is due to Fermi level matching resulting by the electron adsorption. The results demonstrated higher response with regard to NO_2 comparing to other interfering gases denoting its high specific adsorption capability towards NO_2. In the case of NO_2, the higher response could be due to higher high electron-hole ability comparing to other gases. The results revealed maximum response at etching current (15mA/cm^2) around 49.35. The response and the recovery time are considered as an important parameters of the sensing element. The later is regarded as the time

interval taken at the beginning of the gas exposure to the point where the resistance of the sensing element reaches 90% of resistance value. However, the recovery time refers as the time resultant from the moment of gas removal at which the resistance of surface sensing material attains10% of its steady resistance. Tables 3,4 and 5 show the sensitivity, response or recovery time and steady state resistance for SnO_2/PSi thin film at 50°C,100°C and 150°C operating temperature for fixed NO_2 concentration.

The mechanism of gas sensor of the Tin oxide deposited on porous silicon is based on the resistivity change. This result is due to the surrounding air and the gas on the sensor surface in presence the chemical adsorption of oxygen molecules. At the desired operating temperature, the form of oxygen ions on the substrate occurs due to the extraction of electrons from the conduction band of SnO_2/PSi, which acts to an increase in the resistivity of SnO_2/PSi. The adsorbed oxygen mechanism occurs according to the following reactions [29]:

$$O_2(gas) \rightarrow O_2(ads)$$

$$O_2(ads) + e^- \rightarrow O_2^-(ads)$$

$$O_2^-(ads) + e^- \rightarrow 2O^-(ads)$$

$$O^-(ads) + e^- \rightarrow O^{2-}(ads)$$

It is obvious that the Tin oxide is a n- type semiconductor and NO_2 is oxidizing gas, so the reaction of NO_2 with chemically adsorbed oxygen ions on the substrate of SnO_2 works as acceptor and traps the electrons from the SnO_2 NPs. Accordingly, the process yields further increase in the resistance and the barrier height [9,33]. as indicated in the following reactions [33]:

$$NO_2(gas) + e^- \rightarrow NO_2^-(ads)$$
$$NO_2(gas) + O_2^-(ads) + 2e^- \rightarrow NO_2^-(ads) + 2O^-(ads)$$
$$NO_2^-(ads) + O^-(ads) + 2e^- \rightarrow NO(gas) + 2O^{2-}(ads)$$

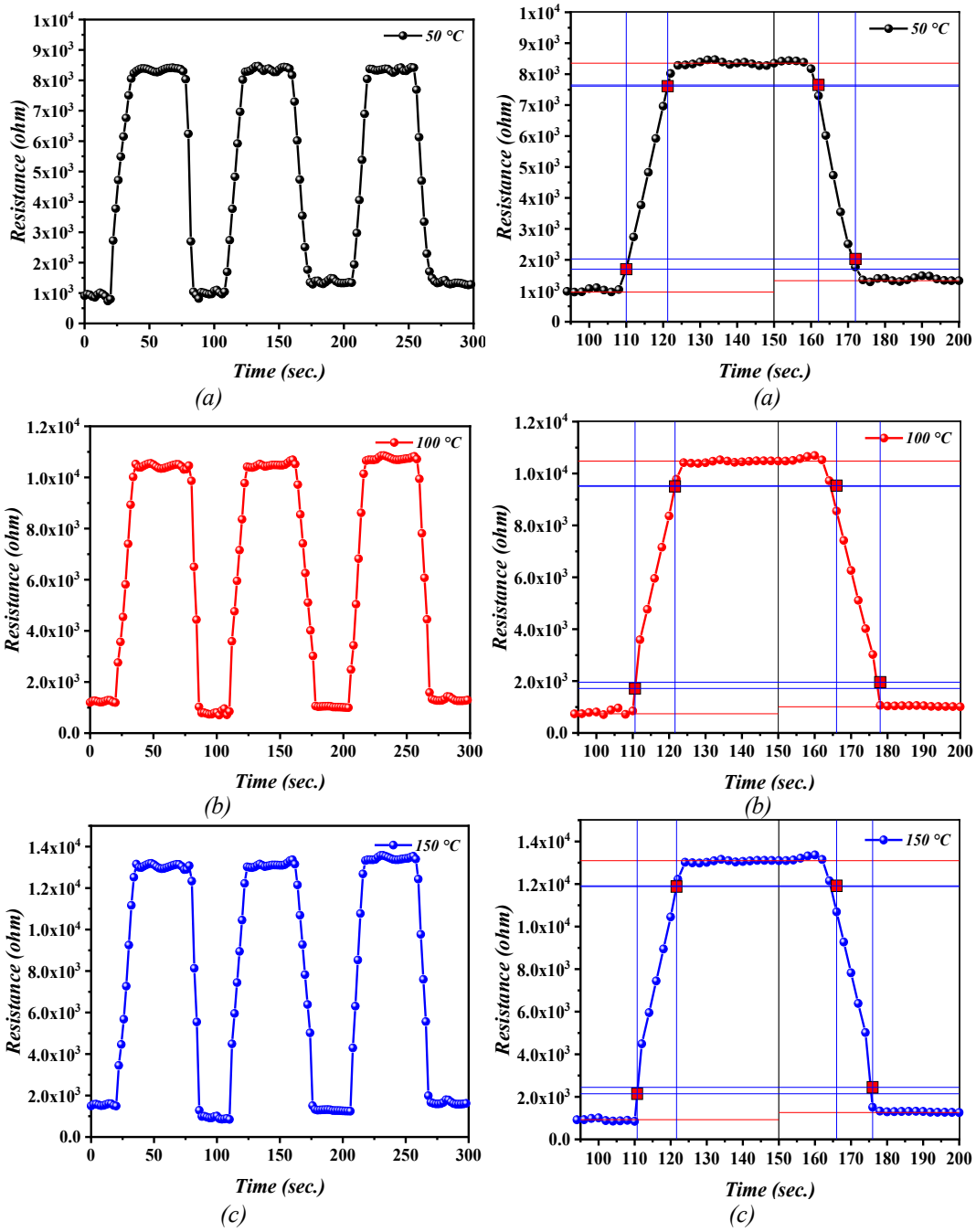

Fig. 8. Switching analysis and Rise and Fall time sensing to 50 ppm of NO_2 gas at (a) 50°C, (b) 100°C, (c) 150°C at etching current density 5mA/cm².

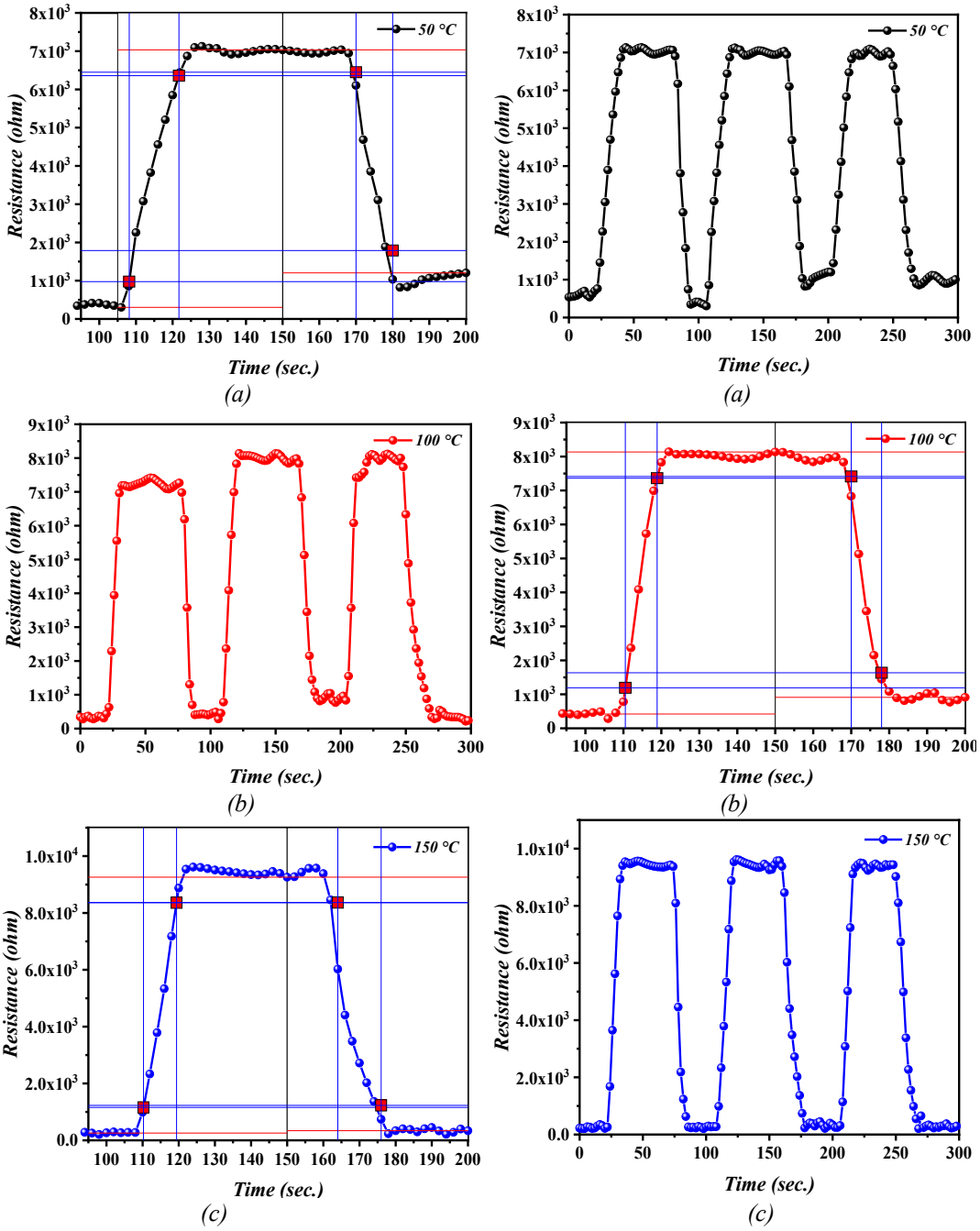

Fig. 9. Switching analysis and Rise and Fall time sensing to 50 ppm of NO_2 gas at (a) 50°C, (b) 100°C, (c) 150°C at etching current density 10mA/cm^2.

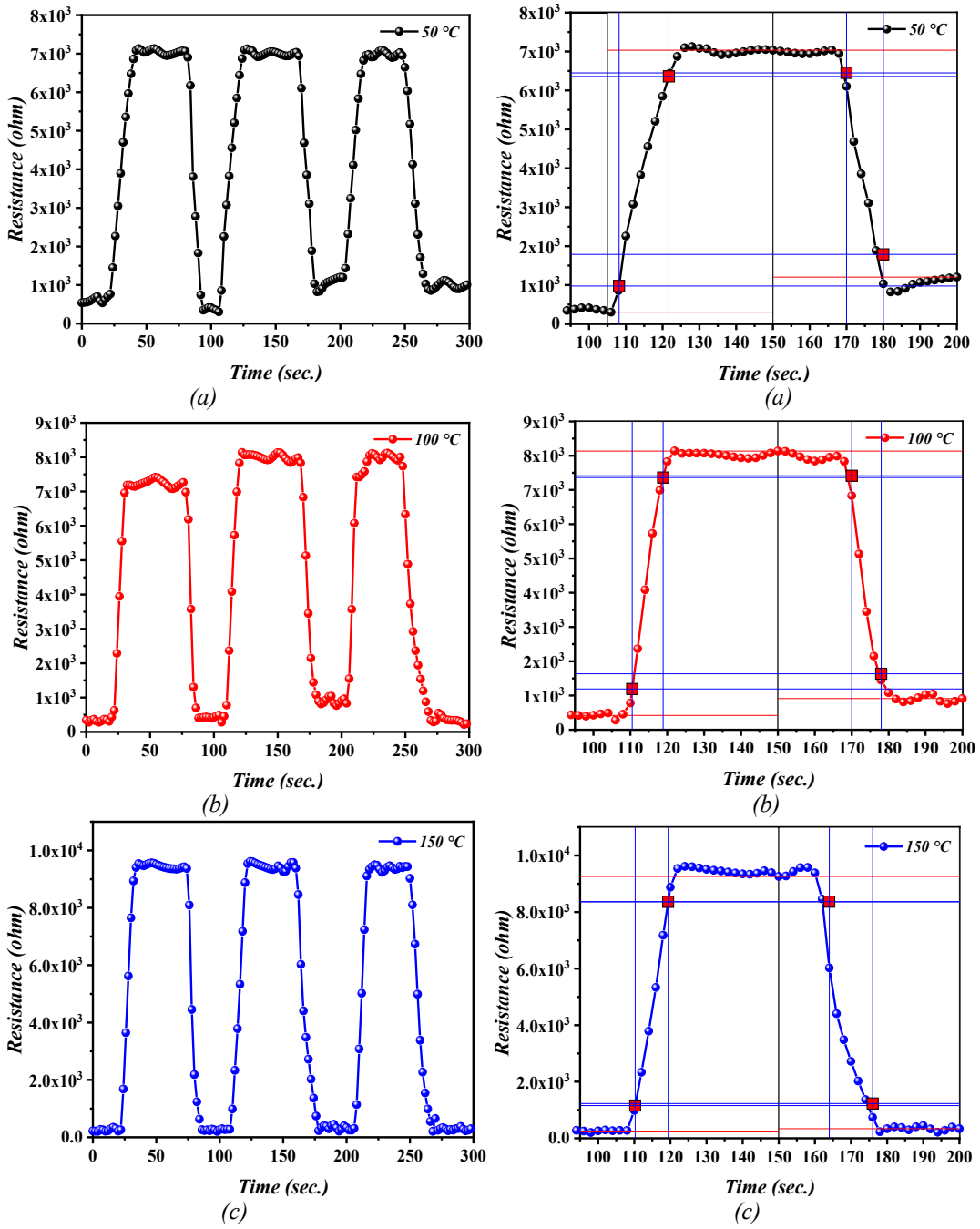

Fig. 10. Switching analysis and Rise and Fall time sensing to 50 ppm of NO_2 gas at (a) 50°C, (b) 100°C, (c) 150°C at etching current density 15mA/cm^2.

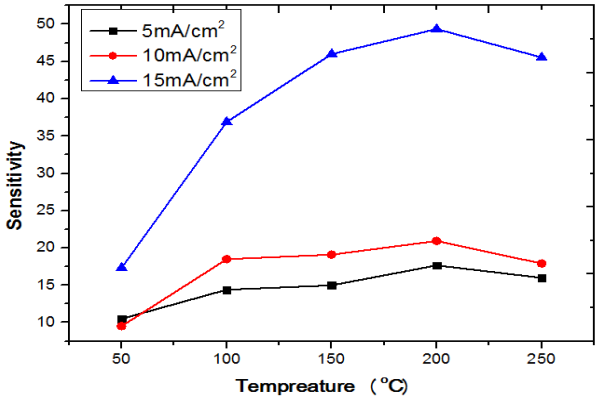

Fig. 11. Sensitivity of the sensor to 50 ppm of NO_2gas as a function of temperature.

Table 3. Summarize of gas sensing to 50 ppm of NO_2 gas at various temperature at 5mA/cm^2.

	50 °C	**100 °C**	**150 °C**	**200°C**	**250°C**
Air	0.735	0.707	0.848	0.893	0.841
Gas	8.47	10.9	13.6	15.76	14.33
G% (NO2)	10.5	14.44	15.0	17.67	16. 0
Response time (Sec)	11.2	10.9	10.9	11.21	10.67
Recovery time (Sec)	10.1	12.8	11.2	11.35	11.26

Table 4. Summarize of gas sensing to 50 ppm of NO_2 gas at various temperature at 10mA/cm^2.

	50 °C	**100 °C**	**150 °C**	**200°C**	**250°C**
Air	0.582	0.502	0.572	0.621	0.592
Gas	6.12	9.80	11.5	13.62	11.21
G% (NO2)	9.51	11.85	19.1	20.93	17.92
Response time (Sec)	13.5	10.1	7.7	7.9	7.3
Recovery time (Sec)	9.6	9.7	9.8	9.9	9.2

Table 5. Summarize of gas sensing to 50 ppm of NO_2 gas at various temperature at 15mA/cm^2.

	50 °C	**100 °C**	**150 °C**	**200°C**	**250°C**
Air	0.303	0.215	0.205	0.195	0.21
Gas	7.13	8.14	9.61	9.82	9.77
G% (NO2)	22.5	36.9	46.0	49.35	45.53
Response time (Sec)	13.5	8.4	9.10	9.32	9.12
Recovery time (Sec)	9.6	9.6	12.4	13.22	12.72

4. Conclusion

In summary, SnO_2 hybrid structure was successfully deposited on porous silicon substrate using spray pyrolysis method. The XRD data exhibit that the SnO_2/PSi NPs was polycrystalline with tetragonal structure. The SEM images confirmed that the SnO_2/PSi have grooves and cavities with average size ranging from 42–64 nm.

The results also indicated that the porous silicon cavities are completely filled by SnO_2 nanostructures. Moreover, the Electrical characteristics revealed a considerable increase in resistivity of the porous layer with etching current density. The data also revealed a degradation in the energy gap of SnO_2 NPs from the values 3.3 to 2.82 eV at spray intervals ranging from 5 to 15 respectively. The results also illustrate a linear increase in the sensitivity of SnO_2/PSi with the etching current. Additionally, the maximum sensing response of 49.35% is found to be around 200℃ for for NO_2 at etching current of value 15mA/cm^2. The sensing approach proposed in this study is straight forward, promising, and cost-effective in the fabrication of high-performance gas sensors.

References

[1] M. H. Younus, G. G. Ali, H. A. Salih,(2021). Journal of Physics: Conference Series, 795,012002, https://doi.org/10.1088/1742-6596/1795/1/012002

[2] G. G. Ali, M. A. Ahmed, A. A. Sulaiman, J. of Nanomaterials and Biostructures ,17, (2022), 473 – 480; https://doi.org/10.15251/DJNB.2022.172.473

[3] T. A. Aswad, T. A. Abbas, G. G. Ali, J. of Nanomaterials and Biostructures 16, (2021), 831 – 838; https://doi.org/10.15251/DJNB.2021.163.831

[4] Y.X. Zhen, B.Y. Song, W.X. Liu, J.X. Ye, X.F. Zhang, Z.P. Deng (2022), 363-131852; https://doi.org/10.1016/j.snb.2022.131852

[5] B.Y. Song, C. Li, M.S. Lv, X.F. Zhang, Z.P. Deng, Y.M. Xu, (2023),387-133811; https://doi.org/10.1016/j.snb.2023.133811

[6] J. Yan, X. Guo, Y. Zhu, Z. Song, L.Y. Lee, J. Mater Chem A. (2022), 10-15657; https://doi.org/10.1039/D2TA03012H

[7] A. Kumar, A.K Shringi, M. Kumar, J. Sensors Actuators B Chem. (2022), 370-132417; https://doi.org/10.1016/j.snb.2022.132417

[8]Rehab Joko Hussin , Ivan B. Karomi,(2024), Silicon , **16**,pp: 5457-5470. https://doi.org/10.1007/s12633-024-03098-2

[9] Y. Kong, Y. Li, X. Cui, L. Su, D. Ma, T. Lai, J. Nanomaterials Mater Science. 4(4), (2022), 339-350; https://doi.org/10.1016/j.nanoms.2021.05.006

[10] Z.P. Li, Q.Q. Zhao, W.L. Fan, J.H. Zhan. (2011), 1646-1652.

[11] C. Nassiri, A. Hadri, F.Z. Chafi, A. El Hat, N. Hassanain, M. Rouchdi, B. Fares,A. Mzerd,. J. Mater Environ Science, 8, (2017), 420-425.

[12] S. Chacko, N.S. Philip, K.G. Gopchandran, P. Koshy, V.K. Vaidyan, M. Tiemann, Chem. Eur J, 13, (2017), 8376-8388; https://doi.org/10.1002/chem.200700927

[13] D. Xue, P. Wang, Z. Zhang, Y. Wang, J. Sensor Actuator B Chem (2019), 126710; https://doi.org/10.1016/j.snb.2019.126710

[14] Y. Cui, Y. Harada, E. Ikenaga, R. Li, N. Nakamura, T. Hatanaka, M. Ando, T. Yoshida, G.-L. Li, M. Oshima, J.Phys Chem. C 120, (2016),10936-10940; https://doi.org/10.1021/acs.jpcc.6b02402

[15] W. Chen, Q. Zhou, T. Gao, X. Su, F. Wan, J. Nanomater (2013),1-9; https://doi.org/10.1155/2013/127345

[16] X.T. Zhou, J.Q. Hu, C.P. Li, D.D.D. Ma, C.S. Lee, S.T. Lee. 369, (2003),220-224. Lett; https://doi.org/10.1016/S0009-2614(02)02008-0

[17] X. Wang, S. Qiu, C. He, G. Lu, W. Liu, J. Liu, 3, (2013), 19002; https://doi.org/10.1039/c3ra43266a

[18] Y.J. Kwon, A. Mirzaei, H.G. Na, S.Y. Kang, M.S. Choi, J.H. Bang, W. Oum, S.S. Kim, H.W. Kim,29, (2018), 294001; https://doi.org/10.1088/1361-6528/aac17b

[19] A. Tischner, T. Maier, C. Stepper, A .Kock, J. Sensors Actuators B, 134, (2008) 796-802; https://doi.org/10.1016/j.snb.2008.06.032

[20] Hwang, I.-S.; Choi, Y.-J., Park, J.-H.; Park, J.-G.; Kim, K.-W.; Lee, J. H., J. Korean Phys. Soc. 49, (2006), 1229-1233

[21] G. Singh, N. Kohli, R.C. Singh, J. of Materials Science Materials in Electronics, 28, (2017), 2257-2266; https://doi.org/10.1007/s10854-016-5796-3

[22] R. Li, J. Sensors and Actuators B Chemical 252,(2017), 79-85; https://doi.org/10.1016/j.snb.2017.05.161

[23] Z. Li, and J. Yi, Sensors and Actuators B: hemical,243,(2017),96-103; https://doi.org/10.1016/j.snb.2016.11.136

[24] D. Han, L. Zhai, F. Gu, Z. Wang, J. Sensors Actuators B Chem. 262, (2018), 655-663; https://doi.org/10.1016/j.snb.2018.02.052

[25] J.M. Walker, S.A. Akbar, P.A. Morris, Sensors Actuators B Chem, 286, (2019), 624-640; https://doi.org/10.1016/j.snb.2019.01.049

[26] H.C. Chiu, C.S. Yeh, J. Phys. Chem. C, 111, (2007), 7256-7259; https://doi.org/10.1021/jp0688355

[27] S. Majumder, S. Hussain, R. Bhar, A.K. Pal, 81, (2007),81 985-996; https://doi.org/10.1016/j.vacuum.2006.12.002

[28] S.-H. Choi, I.-S. Hwang, J.-H. Lee, S.-G. Oh, I.D. Kim, Chem.Commun. 47, (2011),9315-9317; https://doi.org/10.1039/c1cc10707k

[29] J. Zhang, X. Liu, S. Wu, M. Xu, X. Guo, S. Wang, J. Mater Chem, 20, (2010), 6453-6459; https://doi.org/10.1039/c0jm00457j